Role of internal and continuum modes in modulational instability of quadratic solitons

Dmitry V. Skryabin*
Department of Physics and Applied Physics, University of Strathclyde, Glasgow G4 0NG, Scotland
(Received 2 June 1999)

The role of internal and continuum modes in the modulational instability of spatial quadratic solitons is examined by asymptotic and numerical analyses. It is shown that these modes generate novel spatially symmetric and asymmetric modulation instability branches, which underline soliton dynamics throughout a wide region of the wave-vector mismatch. [S1063-651X(99)07912-X]

PACS number(s): 42.65.Tg

I. INTRODUCTION

The evolution of optical solitary waves under the action of a perturbation of different physical origin is one of the active areas of theoretical nonlinear optics. This problem can be tackled using soliton eigenmodes, which are solutions of the associated linear eigenvalue problem. The eigenmodes can be either localized or delocalized with respect to the soliton itself. The former ones are the modes of the discrete spectrum and the latter ones are the modes of the continuum. Stable discrete eigenmodes, or *internal modes* [1], being excited can propagate over very long distances [2]. Their excitations can cause, e.g., periodic oscillations of the soliton width [3–5] or position [6,7]. Resonances of the two internal modes with zero propagation constants always imply a soliton bifurcation which can lead either to stationary instability [3,8–10] or to the appearance of another solitonic branch [10,11]. The resonances of two pairs of the internal modes with nonzero (equal in absolute values and opposite in signs) propagation constants lead to a Hamiltonian-Hopf instability, i.e., instability generated by a pair of complex-conjugated propagation constants [9,12,13]. Internal and continuum modes also cause certain nontrivial effects in the soliton interaction; see, e.g., [11,14]. As one can see from these examples both internal and continuum modes play a very important role practically in all aspects of the soliton dynamics.

Considering experimental schemes for an observation of the spatial self-trapping and soliton generation, high-input-power levels are often required in materials with small nonlinear susceptibilities and/or significant absorbtion. E.g., generation of Kerr and quadratic solitons in planar waveguides requires powers of the order of 1 kW [15,16]. Such powers can be practically easily achieved using pulses; therefore the effect of the group velocity dispersion (GVD) on the propagation of the spatial solitons can become considerable, causing their break up into spatio-temporal clusters via development of the so-called *modulational instability* (MI); see [17–29] and [30–32], respectively, for theoretical and experimental results on the MI of solitons and solitonlike beams and pulses. The instabilities introduced in the preceding paragraph are usually called *internal or longitudinal instabilities* and should be distinguished from MI which is the subject of the present investigation.

GVD-induced MI of the spatial solitons is closely linked with the concept of spatio-temporal solitons, which have been recently observed in an experiment with the bulk quadratically nonlinear medium [33]. It has been shown theoretically that the fully developed MI of the spatial solitons results in the generation of a train of the spatio-temporal quasisolitons [19,20,27]. Growing sidebands in the frequency spectrum of the spatio-temporal pulse propagating in the quadratic medium have also have been observed (see Fig. 3 in [33]), indicating the presence of GVD-induced MI. However, bulk media typically have relatively low GVD and therefore large and controllable GVD coefficients in Bragg structures probably are more promising for the practical utilization of spatio-temporal solitons for all optical processing of information; see, e.g., [34] and references therein.

MI of the solitary waves is often routinely considered as a continuation of the neutrally stable modes of the soliton spectrum at zero modulational frequency Ω, i.e., soliton eigenmodes with zero propagation constants related to system symmetries, into the region $\Omega \neq 0$. However, generally, not only the neutral but also internal and continuum eigenmodes can potentially produce MI branches. An analysis of this problem was largely avoided in the publications on MI of the spatial solitons supported by the quadratic ($\chi^{(2)}$) nonlinearity [22–28] and has also remained a practically untouched issue in the more general solitonic context. It is in sharp contrast with the, already-described, detailed understanding of the influence of the internal modes on the ''internal'' soliton dynamics. Here I will demonstrate the presence of the novel MI branches in the quadratic soliton spectrum, which originate from either internal or continuum modes and influence soliton dynamics throughout a wide physically realistic range of parameters.

II. MODEL EQUATIONS

The evolution of the slowly varying wave envelopes of the first (E_1) and second (E_2) harmonics propagating in the diffractive and dispersive $\chi^{(2)}$ medium under the conditions of type-I phase matching can be described by the following set of the dimensionless equations [22–26]:

$$i\partial_z E_1 + \frac{1}{2}\partial_x^2 E_1 + \gamma_1 \partial_\tau^2 E_1 + E_1^* E_2 = 0,$$

*URL: http://cnqo.phys.strath.ac.uk/~dmitry

$$i\partial_z E_2+\frac{1}{4}\partial_x^2 E_2+\gamma_2\partial_\tau^2 E_2+\frac{1}{2}E_1^2=\beta E_2. \quad (1)$$

Here x is the transverse coordinate measured in units of the characteristic beam width. Definitions of the other parameters and independent variables depend from a particular choice of the experimental scheme, where Eqs. (1) can be applicable. First, Eqs. (1) describe one-transverse-dimensional noncritically phase-matched experimental schemes, where temporal walkoff can be neglected or compensated by some special techniques; see, e.g., [33,35]. Then z is the longitudinal coordinate measured in units of a suitable diffraction length l_{dif}, τ is the dimensionless retarded time, and β is the wave-vector mismatch measured in units l_{dif}^{-1}, which is in the case of quasiphase matching has to be corrected by the grating constant [36]. $|\gamma_1/\gamma_2|$ is the relative strength of the GVDs. If $2\gamma_1=4\gamma_2=1$, then Eqs. (1) also describe propagation in a bulk medium with τ being the second transverse coordinate. Second, considering the degenerate three-wave mixing in a doubly periodic Bragg grating embedded in the quadratic medium He and Drummond [37] and Conti with co-workers [38] have showed that for the frequencies close to the center of the forbidden gap model equations governing propagation dynamics can be reduced to a form which formally coincides with Eqs. (1). The only difference is that temporal and longitudinal coordinates should be interchanged. The reason for this is that in the Bragg gratings the dominating dispersion originates from the delayed spatial, not temporal, response of the medium. More details on renormalization of the dependent and independent variables and parameters can be found in [16,23–26,37,38].

III. ASYMPTOTIC STABILITY ANALYSIS: THE ROLE OF INTERNAL MODES

Equations (1) with $\partial_\tau=0$ have a family of the ground-state solitary solutions $E_m(x,z)=A_m(x)e^{im\kappa z}$ $(m=1,2)$, if $\kappa>\max(0,-\beta/2)$. These solitons can be internally unstable for $\beta<0$ providing that $\partial_\kappa Q<0$ [8], where $Q=\int dx(A_1^2+2A_2^2)$ is the soliton energy.

To study MI of the solitons we seek solutions of Eqs. (1) in the form

$$E_m=\{A_m(x)+[U_m(x,z)+iW_m(x,z)]\cos\Omega t\}e^{im\kappa z}, \quad (2)$$

where $\Omega\geqslant 0$ is the modulation frequency, U_m, W_m are small perturbations, and $m=1,2$. Separating the real and imaginary parts of the linearized problem and setting $U_m\sim u_m(x)e^{\lambda z}$, $W_m\sim w_m(x)e^{\lambda z}$, we obtain two adjoint eigenvalue problems (EVP)

$$-\hat{\mathcal{L}}_0\hat{\mathcal{L}}_1\vec{u}=(\lambda^2+\Omega^2\hat{\gamma}\hat{\mathcal{L}}_1+\Omega^2\hat{\mathcal{L}}_0\hat{\gamma}+\Omega^4\hat{\gamma}^2)\vec{u}, \quad (3)$$

$$-\hat{\mathcal{L}}_1\hat{\mathcal{L}}_0\vec{w}=(\lambda^2+\Omega^2\hat{\gamma}\hat{\mathcal{L}}_0+\Omega^2\hat{\mathcal{L}}_1\hat{\gamma}+\Omega^4\hat{\gamma}^2)\vec{w}, \quad (4)$$

defining the mode structure of the soliton induced linear waveguide. Here $\vec{v}=(u_1,u_2)^T$, $\vec{w}=(w_1,w_2)^T$,

$$\hat{\mathcal{L}}_{0,1}=\begin{pmatrix} -\frac{1}{2}\partial_x^2+\kappa\pm A_2 & -A_1 \\ -A_1 & -\frac{1}{4}\partial_x^2+2\kappa+\beta \end{pmatrix}, \quad (5)$$

$$\hat{\gamma}=\begin{pmatrix} \gamma_1 & 0 \\ 0 & \gamma_2 \end{pmatrix}, \quad (6)$$

and λ is an eigenvalue or, in other words, a propagation constant of a soliton eigenmode.

Let suppose that $\kappa+\gamma_1\Omega^2\equiv\xi_1\geqslant 0$ and $2\kappa+\beta+\gamma_2\Omega^2\equiv\xi_2\geqslant 0$. Then, generally, $\lambda^2\in(-\infty,-\lambda_g^2)$ is a continuous part of the spectrum with unbounded eigenfunctions, where $\lambda_g=\min(\xi_1,\xi_2)$. Eigenvalues which do not belong to the continuum constitute the discrete part of the spectrum and have bounded eigenfunctions. Stable eigenmodes with eigenvalues obeying $-\lambda_g^2<\lambda^2<0$ are the internal modes. Any other mode of the discrete spectrum, i.e., any eigenmode with λ^2 complex or positive, renders the soliton unstable. If $\xi_1<0$ and/or $\xi_2<0$, the gap is closed, $\lambda_g=0$. Phase, translational, and Galilean symmetries and infinitesimal variations of κ allow us to identify zero-eigenvalue (or neutral) eigenmodes of the adjoint operators $\hat{\mathcal{L}}_1\hat{\mathcal{L}}_0$ and $\hat{\mathcal{L}}_0\hat{\mathcal{L}}_1$. These eigenmodes are $\vec{w}_\phi=(A_1,2A_2)^T$, $\vec{w}_v=x(A_1,2A_2)^T$, $\vec{u}_\kappa=\partial_\kappa(A_1,A_2)^T$, and $\vec{u}_x=\partial_x(A_1,A_2)^T$ and they obey following identities: $\hat{\mathcal{L}}_0\vec{w}_\phi=0$, $\hat{\mathcal{L}}_0\vec{w}_v=-\vec{u}_x$, $\hat{\mathcal{L}}_1\vec{u}_\kappa=-\vec{w}_\phi$, and $\hat{\mathcal{L}}_1\vec{u}_x=0$.

Full information about the spectra of EVPs (3) and (4) can be obtained only numerically, but for small absolute values of λ application of an asymptotic approach leads to some analytical predictions. Similarly to the previously studied cases branches of the discrete spectrum produced by the spatially symmetric $\vec{w}_\phi$, $\vec{u}_\kappa$ and by the spatially asymmetric vectors $\vec{w}_v$, $\vec{u}_x$ can be considered independently. A symmetric branch being unstable causes clustering of the solitons into the spatio-temporal patches (neck MI) and an unstable asymmetric branch causes soliton bending (snake MI).

To study discrete spectrum arising due to branching of the symmetric and asymmetric modes it is naturally to consider EVP (4) and (3), respectively. The internal modes are symmetric ones [3] and therefore we focus on the EVP (4) below. We seek its eigenmodes in the form

$$\vec{w}=\vec{w}_\phi+\sum_{j=1}^{+\infty}\vec{w}_j, \quad (7)$$

where $|\vec{w}_j|\sim|\lambda|^{2j}$ and $|\lambda|^2\sim\epsilon\ll 1$. The key difference with previous analyses [22–28] is that we assume here $\Omega^2\sim\epsilon^2$, not $\sim\epsilon$. It allows us to get a balanced equation for λ^2, which takes into account the branching of the both neutral and internal modes.

Substituting Eq. (7) into Eq. (4) one can obtain the following expression for $\vec{w}$:

$$\vec{w}=\vec{w}_\phi+\lambda^2\hat{\mathcal{L}}_0^{-1}\vec{u}_\kappa-\lambda^4\hat{\mathcal{L}}_1^{-1}\hat{\mathcal{L}}_0^{-1}\vec{u}_\kappa-\Omega^2\hat{\gamma}\vec{w}_\phi+O(\epsilon^3). \quad (8)$$

Using the condition

$$\langle(\lambda^2+\Omega^2\hat{\mathcal{L}}_1\hat{\gamma}+\Omega^2\hat{\gamma}\hat{\mathcal{L}}_0+\Omega^4\hat{\gamma}^2)\vec{w}|\vec{u}_\kappa\rangle=0, \tag{9}$$

which holds for any solution of EVP (4), one can get an equation for λ. Brackets $\langle\cdots|\cdots\rangle$ define an inner product in L_2. Equation (9) has asymptotic character and has to be satisfied in each order of ϵ. The first-order condition requires $\lambda^2\partial_\kappa Q\sim\epsilon^2$, implying that the internal instability threshold $\partial_\kappa Q=0$ should be close enough. The second-order condition gives a quadratic equation for λ^2:

$$\Omega^2\langle\hat{\gamma}\vec{w}_\phi|\vec{w}_\phi\rangle=\lambda^2\left(\frac{1}{2}\partial_\kappa Q+\lambda^2 M\right). \tag{10}$$

Here $M=\langle\hat{\mathcal{L}}_0^{-1}\vec{u}_\kappa|\vec{u}_\kappa\rangle$ is the soliton ''mass,'' which was proved to be positive [8].

If the longitudinal instability threshold is far, then $\partial_\kappa Q\sim\epsilon^0$ and one can assume that $|\lambda|^2\sim\Omega^2\sim\epsilon$. In this situation the leading order for λ^2 is

$$\lambda^2=\frac{2\Omega^2\langle\hat{\gamma}\vec{w}_\phi|\vec{w}_\phi\rangle}{\partial_\kappa Q}, \tag{11}$$

which coincides with the previously derived expressions [22,24–26,28]. If point $\partial_\kappa Q=0$ is close, then Eq. (11) has to be used in its full form. This results in

$$\lambda_\pm^2=\frac{1}{2M}\left(-\frac{1}{2}\partial_\kappa Q\pm\sqrt{\frac{1}{4}(\partial_\kappa Q)^2+4M\Omega^2\langle\hat{\gamma}\vec{w}_\phi|\vec{w}_\phi\rangle}\right). \tag{12}$$

At $\Omega=0$, Eqs. (12) give the doubly degenerate zero eigenvalue corresponding to the neutral mode $\vec{w}_\phi$ and the eigenvalues $\pm\sqrt{-\partial_\kappa Q/(2M)}$ corresponding to the internal modes. It is clear that the root λ_+^2 corresponds to the spectral branch produced by the neutral modes and that the root λ_-^2 corresponds to the branch produced by the stable ($\partial_\kappa Q>0$), i.e., internal, or unstable ($\partial_\kappa Q<0$) modes which have nonzero eigenvalues.

There are no spatially asymmetric internal modes and therefore previously obtained analytical results concerning snake MI produced by the translational mode [22–24,28] remain correct throughout an entire soliton existence region. In our notations the corresponding expression for λ^2 is

$$\lambda^2=2\Omega^2\frac{\langle\hat{\gamma}\vec{u}_x|\vec{u}_x\rangle}{Q}. \tag{13}$$

A. Normal GVD-induced MI: $\gamma_{1,2}<0$

Equation (13) indicates that snake MI is always present in this case. Neck MI originating in the neighborhood of $\Omega=0$ is clearly impossible when $\partial_\kappa Q\sim\epsilon^0$. However, if $\partial_\kappa Q\sim\epsilon$, then the low-frequency neck MI becomes possible for either sign of $\partial_\kappa Q$; see Eq. (12).

If $\partial_\kappa Q>0$, then the neck MI starts to grow from

$$\Omega_c^2=\frac{(\partial_\kappa Q)^2}{16M|\langle\hat{\gamma}\vec{w}_\phi|\vec{w}_\phi\rangle|}. \tag{14}$$

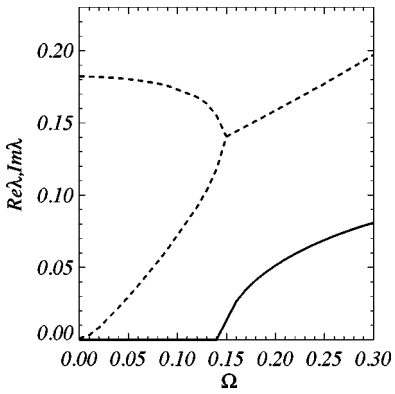

FIG. 1. Bifurcation diagram showing the collision of two gap modes and the onset of the Hamiltonian-Hopf neck-I instability: $\beta=-1.8$, $\kappa=1$, $\gamma_{1,2}=-0.5$.

This is because at $\Omega=\Omega_c$ the square root in Eq. (12) becomes zero, indicating collision of the two eigenvalues λ_+^2 and λ_-^2, corresponding to the two pairs of the internal modes. This collision gives onset to the Hamiltonian-Hopf instability with complex conjugated eigenvalues. If $\partial_\kappa Q<0$, then a similar bifurcation happens at the same Ω_c, with a soliton which was already internally unstable for $\Omega<\Omega_c$.

B. Diffraction and anomalous GVD-induced MI: $\gamma_{1,2}>0$

It follows from Eqs. (11) and (12), that if $\partial_\kappa Q>0$, then only the neutral mode $\vec{w}_\phi$ gives onset to the neck MI and the eigenvalue λ_-^2 corresponding to a pair of the internal modes remains within the gap. The situation is reversed for $\partial_\kappa Q<0$; i.e., the eigenvalue λ_+^2 corresponding to $\vec{w}_\phi$ shifts inside the gap with Ω increasing and λ_-^2 produces a branch of the neck MI. Snake MI generated by the translational mode [see Eq. (13)] does not produce MI branches in this case.

IV. NUMERICAL STABILITY ANALYSIS : THE ROLE OF CONTINUUM MODES

The MI spectrum in the region of large Ω and, in particular, the study of the possible splitting of MI branches from the continuum can be most straightforwardly done using numerical methods. To address these problems, the EVP (4) has been solved numerically using second-order finite differences. A direct simulation of Eqs. (1) has also been performed to compare with the results of the linear approach.

A. Normal GVD-induced MI: $\gamma_{1,2}<0$

Let us note from the very beginning that for different values of β numerical results reveal the presence of as many as three branches of neck-type and two branches of snake-type MI. We will gradually introduce all five branches, starting our consideration from the parameter region where $\partial_\kappa Q\sim\epsilon$ and asymptotic expression (12) can be applied. First we have numerically verified the appearance of the Hamiltonian-Hopf neck instability for $\Omega>\Omega_c$. The corresponding bifurcation diagram is shown in Fig. 1. The MI branch originating from this bifurcation will be below called neck-I MI.

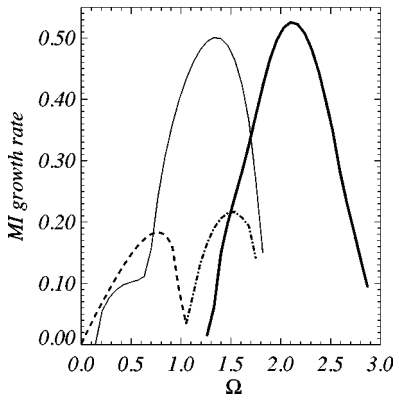

FIG. 2. MI growth rates vs Ω for $\kappa=1$, $\beta=-1.8$, $\gamma_{1,2}=-0.5$. The thin solid line corresponds to the neck-I MI with complex eigenvalues, the bold solid line to the neck-II MI with real eigenvalue, the dashed line to the snake-I MI with real eigenvalues, and the dash-dotted line to the snake-II MI with complex eigenvalues.

For normal GVD the gap in the continuous spectrum narrows with increasing of Ω and it closes at $\Omega_g^2=\min(\kappa/|\gamma_1|,(2\kappa+\beta)/|\gamma_2|)$. With a further increase of Ω the growth rate of the neck-I MI approaches its maximum, then decays, and finally disappears inside the continuum at some $\Omega>\Omega_g$; see solid line in Fig. 2. Slightly before this point but after the closure of the gap another branch of the discrete spectrum with purely real eigenvalues, neck-II MI, splits from the continuum. Though the neck-I branch shown in Fig. 2 looks like it consists of two independent MI bands, numerical results indicate that at these parameter values it is a single branch. However, with β increasing, approximately at $\beta\simeq-1$, it indeed splits into two independent branches with the associated eigenvalues being complex numbers. The low-frequency band will be called neck-III MI and the high-frequency band inherits the name neck-I MI. The scenario of the appearance of neck-III MI changes with increasing β. The internal soliton modes at $\Omega=0$ disappear inside the continuum for $\beta>0$ [3], and the neck-III branch splits directly from the edge of the continuum when the eigenvalue associated with $\vec{w}_\phi$ approaches this edge [39]. Considering the appearance of neck-I MI, after the splitting into the two bands, numerical results unambiguously reveal that now this branch splits directly from the continuum. The first band of snake MI, snake-I, is linked to the translational mode [see Eq. (13)], and the second band, snake-II, bifurcates from the continuum having complex conjugated eigenvalues. These two bands are also shown in Fig. 2.

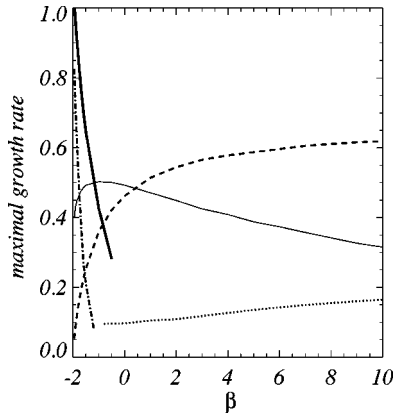

FIG. 3. Maximal MI growth rates [40] vs β for $\kappa=1$, $\gamma_{1,2}=-0.5$. Neck-I MI, thin soild line; neck-II MI, bold solid line; neck-III MI, dotted line; snake-I MI, dashed line; snake-II MI, dash-dotted line.

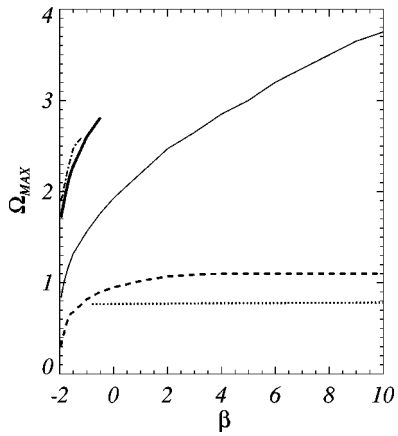

FIG. 4. Maximally unstable frequencies $\Omega_{\max}$ [40] vs β. Parameters and notation the same as in Fig. 3.

Close to the internal stability threshold $\partial_\kappa Q=0$, the maximal growth rates [40] of the secondary MI branches, neck-II and snake-II, occur at the frequencies which are approximately twice the maximally unstable frequencies of the primary instabilities, neck-I and snake-I, linked to the neutral and internal modes; see Fig. 2. This indicates the importance of the second temporal harmonic in the development of MI in the region $\partial_\kappa Q\sim\epsilon$ where the second harmonic of the soliton itself is dominant over or comparable with the fundamental field. Increasing β leads to the suppression of the second harmonic field and therefore the neck-II and snake-II instabilities quickly decay and finally disappear. Figure 3 and 4 illustrate, respectively, how the maximal growth rates and maximally unstable modulation frequency $\Omega_{\max}$ of all five MI branches depend on β. Thus one can see that snake-I MI dominates the soliton dynamics for $\beta>0.5$ and that for $\beta<0.5$ the dominating instabilities are neck-I or neck-II. The soliton spectrum for sufficiently large β is shown in Fig. 5.

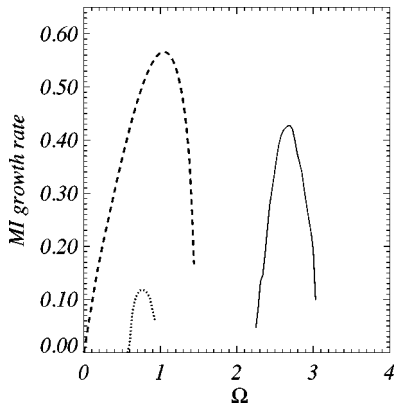

FIG. 5. MI growth rates vs Ω for $\kappa=1$, $\beta=3$, $\gamma_{1,2}=-0.5$. The solid line corresponds to the neck-I MI, the dotted line to the neck-III MI, and the dashed line to the snake-I MI.

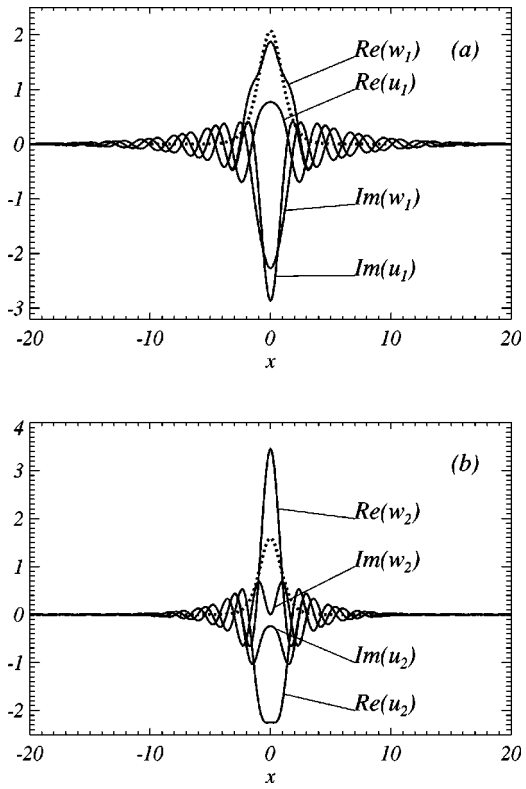

FIG. 6. Typical spatial profiles of the eigenvectors corresponding to the neck-I MI: $\gamma_{1,2}=-0.5$, $\kappa=1$, $\beta=-1$, $\Omega=1.9$. Dotted lines mark corresponding profiles of the solitary waves. (a) Fundamental field; (b) second-harmonic field.

Typical profiles of the most unstable eigenmodes corresponding to neck-I MI are shown in Fig. 6. Weakly damped oscillatory tails of these modes unambiguously verify the link of this MI branch with the continuous spectrum. The results of the direct numerical simulation of Eqs. (1) with initial conditions in the form of a soliton stripe perturbed only by noise supporting the presented stability analysis are shown in Figs. 7–9. Note that not only for $\beta\sim 0.5$, but practically throughout all the range of possible mismatches, several MI branches underline the soliton evolution. E.g., the snake-I MI is dominant for the large positive β, but the neck-type dynamics can be clearly seen in the second harmonic field; see Figs. 9(a_2) and 9(b_2).

B. Diffraction and anomalous GVD-induced MI: $\gamma_{1,2}>0$

Numerical investigation of EVP (4) indicates that in this case MI branches predicted by the asymptotic analysis are only unstable branches of the spectrum; see Sec. III B. In the case $\partial_\kappa Q>0$, an initially uniform stripe develops into a multihump structure with each hump forming a quasistable spatio-temporal filament oscillating upon propagation. Such a scenario is a typical one not only for the quadratic solitons (see [24–28]), but also for the solitons in media with a saturable nonlinearity [20]. The problem of MI of the longitudinally unstable solitary stripe, $\partial_\kappa Q<0$, looks more subtle. However, the longitudinal instability ($\Omega=0$) appears to be suppressed by the MI ($\Omega_{\max}\neq 0$), resulting in a dynamics similar to the longitudinally stable case [24–28].

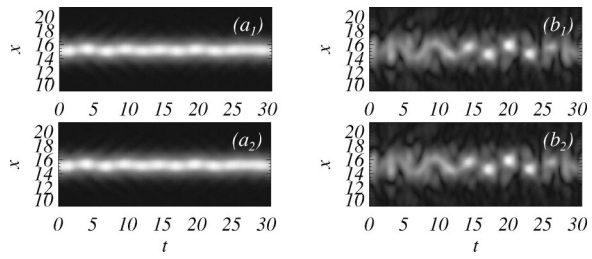

FIG. 8. Competition between neck and snake instabilities. Neck-I and snake-I instabilities have approximately equal growth rates. $\kappa=1$, $\beta=0$, $\gamma_{1,2}=-0.5$. ($a_{1,2}$) $|E_{1,2}|$ at $z=10$, ($b_{1,2}$) $|E_{1,2}|$ at $z=15$.

V. SUMMARY AND DISCUSSION

Asymptotic and numerical analyses revealing the very important role played by the internal and continuum eigenmodes in the modulational instability of quadratic solitons in the type-I phase matching geometry have been performed. It is demonstrated that the neck-type instability induced by the normal GVD of both harmonics and dominating soliton dynamics throughout the region of the negative wave-vector mismatch originates from bifurcations involving the internal and continuum modes. The snake instability causing soliton bending and studied previously in detail in Refs. [23,24] was found to compete with the neck instability in the entire region of the soliton existence.

Internal modes of one-dimensional (1D) type-I quadratic solitons can be considered as one of their striking features compare to 1D Kerr solitons. Although solitons in both these models have the same set of the neutral modes, the importance of the internal modes manifests itself in the existence of neck MI of the quadratic solitons in the media with normal GVD. Internal modes are particularly important when they are close the resonance with the neutral ones. Thus the part of the presented results dealing with the internal modes

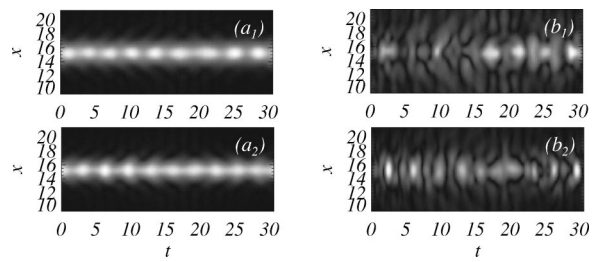

FIG. 7. Competition between neck and snake instabilities. Snake instabilities are suppressed. $\kappa=1$, $\beta=-1$, $\gamma_{1,2}=-0.5$. ($a_{1,2}$) $|E_{1,2}|$ at $z=10$, ($b_{1,2}$) $|E_{1,2}|$ at $z=15$.

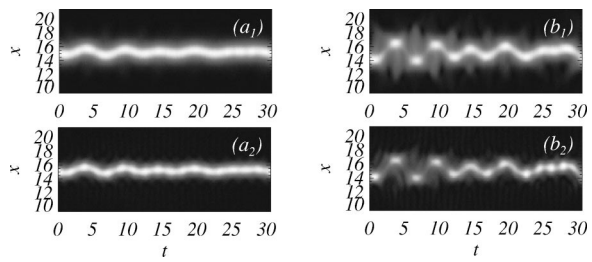

FIG. 9. Competition between neck and snake instabilities. Snake-I instability is a dominant. $\kappa=1$, $\beta=5$, $\gamma_{1,2}=-0.5$. ($a_{1,2}$) $|E_{1,2}|$ at $z=10$, ($b_{1,2}$) $|E_{1,2}|$ at $z=12$.

can be compared with the competition of the neck and snake instabilities of the *vector* solitons in Kerr [29] and type-II quadratic [28] media, where this phenomenon and the associated higher degeneracy of the zero soliton eigenvalue originate from an extra phase symmetry. Neck-type MI branches linked to the internal and continuum modes can also be found in the type-II case, but they are mostly suppressed by the MI due to the extra phase symmetry [28].

The quadratic equation for eigenvalues of the spatially symmetric eigenmodes similar to Eq. (10) have been derived not only in [28,29], but also in [18,21] in the context of the 2D NLS equation, where an extra degeneracy of the zero eigenvalue is linked with Talanov lens symmetry. Competition between the neck and snake instabilities is also possible in the latter example, but it has not been studied yet. Let me stress that the degeneracy due to symmetries does not depend on the system parameters unlike the degeneracy due to the internal modes, which happens for some critical values of the parameters. Note that the disappearance of the snake MI of the type-I quadratic solitons for the negative wave-vector mismatch has been briefly mentioned in [23]. However, it was left without any details there as well as in the subsequent paper [24].

While the snake MI with spatially asymmetric eigenmodes is a typical solitonic phenomenon, analogs of the neck MI can be traced in MI spectrum of the plane-wave solution, as happens, e.g., for vector-Kerr solitons [29]. In the present context, the MI of the plane-wave solution [$E_1 = \sqrt{2\kappa(2\kappa+\beta)}e^{i\kappa z}$, $E_2 = \kappa e^{i2\kappa z}$] has been studied in [41–43]. The results of these papers have been reproduced putting $\partial_x^2 = 0$ in Eqs. (5). It has been found that clear counterparts of the neck-II and neck-III branches exist, while an important neck-I branch appears to be a purely solitonic effect similarly to the snake instabilities.

The rescaled MI growth rate λ and frequency Ω can be related to their real world values using the formulas $\lambda_{ph} \simeq \lambda/(kw^2)$, $\Omega_{ph}^2 \simeq 2\Omega^2/(k|k''|w^2)$, where λ_{ph} and Ω_{ph} are the growth rate and frequency in physical units, k is the wave number of the fundamental field, w is the characteristical beamwidth, and $k'' = \partial_\omega^2 k(\omega) \simeq \partial_\omega^2 k(2\omega)$ is the GVD parameter. Taking $w \sim 50$ μm, $k \sim 6\times 10^6 m^{-1}$, and $k'' \sim 10^{-24}$ s^2/m [16,42], one will obtain $\lambda_{ph} \simeq \lambda/(1.5$ cm) and $\Omega_{ph} \simeq \Omega/(35$ fs). Thus growing bands in the soliton spectrum should be observable after propagation throughout typical 2–3-cm-long samples. Fully developed neck MI in media with normal GVD should result in the generation of a train of the spatio-temporal solitons. E.g., the 90-ps pulses used in [16] should break up into around 1000 90-fs pulses after propagation of ~ 10 diffraction lengths. However, this is more difficult to observe experimentally because it requires more than 10-cm-long samples. Note that the estimation for the soliton temporal duration is consistent with recent experiments [33]. Well-pronounced pulse position oscillations of the order of the soliton width due to domination of snake MI should appear after propagation of the same distance in media with normal GVD.

Among the soliton MI-related problems which are still open I would like to mention the importance of accounting for the finite size of the pulse Δ in the case when the condition $\Delta\Omega_{\max} \gg 1$ is weakening. The first details of this issue have been recently reported in [26] in the context of diffraction-induced MI. Obviously, the possibilities to have different signs of $\gamma_{1,2}$ and to vary $|\gamma_1/\gamma_2|$ also open doors for the more extensive investigation. However, selective numerical checks have showed that the above-presented study captures most of the qualitatively distinct features originating from bifurcations involving internal and continuum modes.

ACKNOWLEDGMENT

The author acknowledges financial support from the Royal Society of Edinburgh and British Petroleum.

[1] Y.S. Kivshar, D.E. Pelinovsky, T. Cretegny, and M. Peyrard, Phys. Rev. Lett. **80**, 5032 (1998).
[2] D.E. Pelinovsky, Physica D **119**, 301 (1998).
[3] C. Etrich, U. Peschel, F. Lederer, B.A. Malomed, and Y.S. Kivshar, Phys. Rev. E **54**, 4321 (1996).
[4] D.E. Pelinovsky, J.E. Sipe, and J. Yang, Phys. Rev. E **59**, 7250 (1996).
[5] V.V. Afanasjev, P.L. Chu, and Y.S. Kivshar, Opt. Lett. **22**, 1388 (1997).
[6] T. Ueda and W.L. Kath, Phys. Rev. A **42**, 563 (1990).
[7] B.A. Malomed and R.S. Tasgal, Phys. Rev. E **58**, 2564 (1998).
[8] D.E. Pelinovsky, A.V. Buryak, and Y.S. Kivshar, Phys. Rev. Lett. **75**, 591 (1995).
[9] D.V. Skryabin, Physica D (to be published).
[10] E.A. Ostrovskaya, Y.S. Kivshar, D.V. Skryabin, and W.J. Firth, Phys. Rev. Lett. **83**, 296 (1999).
[11] B.A. Malomed, J. Opt. Soc. Am. B **9**, 2075 (1992).
[12] I.V. Barashenkov, D.E. Pelinovsky, and E.V. Zemlyanaya, Phys. Rev. Lett. **80**, 5117 (1998).
[13] A. De Rossi, C. Conti, and S. Trillo, Phys. Rev. Lett. **81**, 85 (1998).
[14] A.V. Buryak, Phys. Rev. E **52**, 1156 (1995).
[15] J.U. Kang, J.S. Aitchison, G.I. Stegeman, and N. Akhmediev, Opt. Quantum Electron. **30**, 649 (1998).
[16] R. Schiek, Y. Baek, G. Stegeman, and W. Sohler, Opt. Quantum Electron. **30**, 861 (1998).
[17] V.E. Zakharov, Zh. Éksp. Teor. Fiz. **53**, 1735 (1967) [Sov. Phys. JETP **26**, 994 (1968)].
[18] V.E. Zakharov and A.M. Rubenchik, Zh. Éksp. Teor. Fiz. **65**, 997 (1973) [Sov. Phys. JETP **38**, 494 (1974)].
[19] N.N. Akmediev, V.I. Korneev, and R.F. Nabiev, Opt. Lett. **47**, 1358 (1993).
[20] N. Akhmediev and J.M. Soto-Crespo, Phys. Rev. A **47**, 1358 (1993).
[21] L. Berge and J.J. Rasmussen, Phys. Plasmas **3**, 824 (1996).
[22] A.A. Kanashov and A.M. Rubenchik, Physica D **4**, 122 (1981).
[23] A. De Rossi, S. Trillo, A.V. Buryak, and Y.S. Kivshar, Opt. Lett. **22**, 868 (1997).
[24] A. De Rossi, S. Trillo, A.V. Buryak, and Y.S. Kivshar, Phys. Rev. E **56**, R4959 (1997).
[25] D.M. Baboiu and G.I. Stegeman, Opt. Lett. **23**, 31 (1998).
[26] D.M. Baboiu and G.I. Stegeman, Opt. Quantum Electron. **30**, 937 (1998).

[27] D.V. Skryabin and W.J. Firth, Opt. Commun. **148**, 79 (1998).
[28] D.V. Skryabin and W.J. Firth, Phys. Rev. Lett. **81**, 3379 (1998).
[29] D.V. Skryabin and W.J. Firth, Phys. Rev. E **60**, 1019 (1999).
[30] R.A. Fuerst, D.M. Baboiu, B. Lawrence, W.E. Torruellas, G.I. Stegeman, S. Trillo, and S. Wabnitz, Phys. Rev. Lett. **78**, 2756 (1997).
[31] J.K. Ranka, R.W. Schirmer, and A.L. Gaeta, Phys. Rev. Lett. **77**, 3783 (1996).
[32] A.A. Zozulya, S.A. Diddams, A.G. Van Engen, and T.S. Clement, Phys. Rev. Lett. **82**, 1430 (1999).
[33] X. Liu, L.J. Qian, and F.W. Wise, Phys. Rev. Lett. **82**, 4631 (1999).
[34] B.J. Eggleton, C.M. de Sterke, and R.E. Slusher, J. Opt. Soc. Am. B **16**, 587 (1999).
[35] P. Di Trapani, D. Caironi, G. Valiulius, A. Dubietis, R. Danielis, and A. Piskarkas, Phys. Rev. Lett. **81**, 570 (1998).
[36] M.M. Fejer, G.A. Magel, D.H. Jundt, and R.L. Byer, IEEE J. Quantum Electron. **28**, 2631 (1992).
[37] H. He and P.D. Drummond, Phys. Rev. Lett. **78**, 4311 (1997).
[38] C. Conti, S. Trillo, and G. Assanto, Phys. Rev. Lett. **78**, 2341 (1997).
[39] The author has to admit that within the accuracy of the numerical method used it was not possible to exclude definitely splitting of an internal mode from the continuum into the gap just before the continuation of the $\vec{w}_\phi$ mode collides with the gap edge.
[40] The maximal growth rate of each particular branch of the soliton spectrum has been found numerically using the condition $\partial_\Omega \mathrm{Re}\,\lambda = 0$. The corresponding value of Ω is $\Omega_{\max}$. For given parameters γ_m, κ, and β several $\Omega_{\max}$ values generally exist (see Figs. 2–5) due to the presence of several modulationally unstable frequency bands.
[41] A.V. Buryak and Y.S. Kivshar, Phys. Rev. A **51**, R41 (1995).
[42] S. Trillo and P. Ferro, Opt. Lett. **20**, 438 (1995).
[43] H. He, P.D. Drummond, and B.A. Malomed, Opt. Commun. **123**, 394 (1996).